Room temperature lithium polymer batteries based on ionic liquids

G.B. Appetecchi [a,*], G.T. Kim [a,b], M. Montanino [a], F. Alessandrini [a], S. Passerini [b,**]

[a] UTRINN-IFC, ENEA (Agency for New Technologies, Energy and Sustainable Economic Development), Via Anguillarese 301, Rome 00123, Italy
[b] Institut fur Physikalische Chemie, Westfälische Wilhelm Universität, Corrensstr. 28/30, Münster D48149, Germany

ARTICLE INFO

ABSTRACT

In this manuscript are reported the results of an investigation performed on rechargeable, all-solid-state, solvent-free, Li/LiFePO$_4$ polymer batteries incorporating N-butyl-N-methyl-pyrrolidinium bis(trifluoromethanesulfonyl)imide, PYR$_{14}$TFSI, ionic liquid (IL). The tests show clearly the beneficial effect due to the incorporation of ionic liquids on room temperature battery performance that, conversely, results extremely poor in IL-free lithium polymer batteries. The theoretical capacity is delivered at 30 °C whereas about 115 mA h g^{-1} are discharged at 20 °C with excellent capacity retention and high coulombic efficiency. At 40 °C large capacities (125 mA h g^{-1}) are discharged even at medium rates (C/3). Impedance measurements revealed that the overall battery resistance is almost fully located (e.g., above 93%) at the lithium anode/polymer electrolyte interface, which plays a key role in determining the battery performance.

1. Introduction

Rechargeable, lithium metal polymer batteries (LMPBs) are indicated as an excellent choice as next generation electrochemical power sources since their high energy density, good cyclability, flexible characteristics and safety [1–5]. In particular, poly(ethyleneoxide)-lithium salt, PEO–LiX, complexes are considered good candidates as electrolyte separators for all-solid-state, LMPB applications [6–10]. Large research efforts have been devoted to the development of PEO electrolyte formulations capable to combine high conductivity, good interfacial stability with lithium metal anode, and good mechanical properties [11–14]. Nevertheless, the room temperature performance of LMPBs is still limited by the low ionic conductivity of the solvent-free PEO-based electrolyte. Conductivity values suitable for practical applications (>10^{-4} S cm^{-1}) are approached only at temperatures higher than 70 °C (above the PEO melting point), i.e., when the polymer is in the amorphous state [15].

A common approach is the use of a lithium salt having a very large counter-ion [e.g., LiN(SO$_2$CF$_3$)$_2$ (LiTFSI), LiN(SO$_2$CF$_2$CF$_3$)$_2$ (LiBETI)], which is able to interfere with the crystallization process of the polymer chains [12,16–18], thereby promoting amorphous regions and increasing the lithium ion transport in the polymer electrolyte [9,17,19]. However, despite an increase of more than one order of magnitude with respect to other common lithium salts [20], the room temperature ionic conductivity is still low (e.g., 10^{-6} S cm^{-1}) for practical applications.

A very promising approach for overcoming this drawback is represented by the incorporation of room temperature ionic liquid (RTILs) into the polymer electrolytes. RTILs are molten salts at room temperature that generally consist of an organic cation and an inorganic/organic anion. The main advantages of RTILs towards organic solvents are: non-flammability, negligible vapor pressure, high chemical, electrochemical and thermal stability and, in some cases, hydrophobicity. RTILs based on saturated, cyclic, quaternary ammonium cations as pyrrolidinium and bis(trifluoromethanesulfonyl)imide (TFSI) as the anion have been proposed for use in lithium batteries since their sub-ambient melting temperature, high room temperature conductivity, suitable electrochemical stability [21]. This latter characteristic originates from the absence of acidic protons and double bounds that strongly deplete the electrochemical stability and compatibility with the lithium metal anode [21,22].

In the last few years, we have successfully demonstrated [23–29] that the addition of N-alkyl-N-methyl-pyrrolidinium bis(trifluoromethanesulfonyl)imide, PYR$_{1A}$TFSI (alkyl = propyl, n-butyl, iso-butyl and n-pentyl), RTILs to solid, PEO-based electrolytes (SPEs) enhances the ionic conductivity above 10^{-4} S cm^{-1} at 20 °C with a wide electrochemical stability and good compatibility towards the lithium anode even after prolonged storage times. Also, the addition of RTILs resulted affecting the Li/SPE interfacial resistance. Successively, the characterization of

$P(EO)_{10}LiTFSI–PYR_{1A}TFSI$ polymer electrolytes has been extended to full $Li/LiFePO_4$ cells [30] which showed very promising performance, in terms of capacity and cycle life, at near room temperature (>30 °C).

In the frame of this work, RTIL-containing $Li/LiFePO_4$ batteries have been optimized in terms of component materials and manufacturing process in order to improve the room temperature performance. $P(EO)_{10}LiTFSI–PYR_{14}TFSI$ electrolyte films, selected on the basis of their electrochemical characteristics [29], were used as the separators in all-solid-state, vacuum-sealed cells that were investigated from 20 °C through 40 °C at current rates ranging from C/50 to 2C. The results are reported in the present paper.

2. Experimental

2.1. Synthesis of the ionic liquid

The N-butyl-N-methylpyrrolidinium bis(trifluoromethanesulfonyl)imide, $PYR_{14}TFSI$, ionic liquid was synthesized through a procedure developed at ENEA [31,32].

2.2. Preparation of the polymer electrolyte and the composite cathode

A solvent-free, hot-pressing process developed at ENEA [23,25,26,29] was used to prepare the $PYR_{14}TFSI$-based PEO electrolyte and the composite cathode. The process was performed in a very low relative humidity dry-room (R.H. < 0.1% at 20 °C). Prior to use LiTFSI (3 M) and $PYR_{14}TFSI$ were dried under vacuum at 120 °C for 24 h while PEO (DOW, WSR 301, MW = 4,000,000) was dried under vacuum at 50 °C for 48 h. PEO and LiTFSI (EO/Li mole ratio = 10) were intimately mixed in a mortar and, then, $PYR_{14}TFSI$ was added to achieve a $(PYR_{14})^+/Li^+$ mole ratio equal to 1. Previous work [26,29,30] has shown that this ratio represents a right compromise between a high ionic conductivity and a good lithium metal interfacial stability. The $P(EO)_{10}LiTFSI–PYR_{14}TFSI$ past-like mixture was annealed under vacuum at 100 °C overnight. Finally, the so-obtained homogeneous, rubber-like material was hot-pressed at 100 °C for 2 min to form 70 to 80 μm thick films.

The cathode tape was prepared by intimately blending $LiFePO_4$ active material (Sud Chemie) and KJB carbon (Akzo Nobel). Before use, $LiFePO_4$ and KJB were dried under vacuum at 110 °C for at least 24 h. Separately, PEO, LiTFSI and $PYR_{14}TFSI$ were mixed to obtain a paste-like mixture that was added to the previous blend. The resulting mixture was firstly annealed at 100 °C overnight and, then, hot-pressed to form preliminary films (200–300 μm thick) that were cold-calendered to obtain the final cathode tape (<50 μm). In addition, the last step allowed removing any porosity within the composite cathode [33]. Finally, 12 mm diameter cathode discs (active area equal to 1.13 cm²) were punched for the battery tests. The final weight composition was $LiFePO_4$:KJB:PEO:LiTFSI:$PYR_{14}TFSI$ = 43.0:7.0:17.5:5.0:27.5. Following the above solvent-free procedure route, RTIL-free cathodes, having $LiFePO_4$:KJB:PEO:LiTFSI = 43.0:7.0:38.9:11.1 (i.e., EO/Li mole ratio = 10) as the final composition, were prepared for comparison purpose. The active material mass loading ranged from 4 mg cm⁻² to 5 mg cm⁻², corresponding to a capacity from 0.7 mA h cm⁻² to 0.8 mA h cm⁻².

2.3. Cell assembly

The electrochemical measurements on the PEO–LiTFSI–$PYR_{14}TFSI$ ternary polymer electrolyte were performed on two-electrode cells fabricated in the dry-room. Three different kinds of cells (active area equal to 1.13 cm²) were assembled for the different measurements by sandwiching a PEO electrolyte layer between: two lithium foil electrodes (chemical stability measurements); two $LiFePO_4$ composite electrodes ($LiFePO_4$/SPE interfacial resistance measurements); and a nickel foil electrode (working electrode; 0.10 mm thick) and a lithium foil electrode (linear sweep voltammetry tests). In the latter kind of cell a tiny lithium strip was used as the reference electrode. The lithium foil used for all cell was 0.05 mm thick.

The solid-state $Li/LiFePO_4$ batteries (cathode limited) were fabricated (inside the dry-room) by laminating a lithium foil (50 μm thick), a $P(EO)_{10}LiTFSI–PYR_{14}TFSI$ polymer electrolyte separator and a $LiFePO_4$-based composite cathode tape. Aluminum and copper grids were used as the cathodic and anodic current collector, respectively. The electrochemical active area of the $Li/LiFePO_4$ cells was 1.13 cm².

All the assembled cells were evacuated for at least 1 h (10⁻² mbar), housed in vacuum-sealed, soft envelopes and, finally, laminated twice by hot-rolling at 100 °C.

2.4. Electrochemical tests

The electrochemical stability window (ESW) of the $P(EO)_{10}LiTFSI–PYR_{14}TFSI$ polymer electrolyte was evaluated by linear sweep voltammetries (LSVs) at 0.5 mV s⁻¹. The measurements were performed scanning the cell potential from the open circuit value (OCV) towards more negative or positive potentials to determine the cathodic and anodic electrochemical stability limits, respectively. The LSVs were performed at least twice on each electrolyte sample to confirm the results obtained using fresh samples and clean electrodes for each test. The measurements were performed at 20 °C using a Schlumberger (Solartron) Electrochemical Interface (model 1287) controlled by software developed at ENEA.

The AC measurements on symmetrical Li/Li and $LiFePO_4/LiFePO_4$ polymer cells (65 kHz–10 mHz) and $Li/LiFePO_4$ LMPBs (10 kHz–10 mHz) were performed in the 20–40 °C temperature interval by means of a F.R.A. Schlumberger Solartron 1260 (controlled by software developed at ENEA) coupled with a Schumberger Solartron Electrochemical Interface 1287. During the experiments the cells were located in a cold/heat test chamber Binder GmbH MK53 with a temperature control of ±0.1 °C.

The cycling performance of the full $Li/LiFePO_4$ batteries were evaluated under charge/discharge rates ranging from C/50 ($j = 0.013$ mA cm⁻²) to 2C ($j = 1.3$ mA cm⁻²) in the 20–40 °C temperature interval. The battery tests were performed using a MACCOR S4000 battery tester. The voltage cut-offs were fixed at 4.0 V (charge step) and 2.0 V (discharge step), respectively.

3. Results and discussion

3.1. PEO–LiTFSI–$PYR_{14}TFSI$ polymer electrolyte

The incorporation of $PYR_{14}TFSI$ ionic liquid leads to a relevant improvement of the chemical and electrical properties of PEO–LiX solid polymer electrolytes (SPEs). In Table 1 are reported the conductivity values of $P(EO)_{10}LiCF_3SO_3$ (from Ref. [20]), $P(EO)_{10}LiTFSI$ [29] and $P(EO)_{10}LiTFSI–PYR_{14}TFSI$ [29] polymer electrolytes at different temperatures. The data clearly show the beneficial effect due to the large size anion lithium salt (TFSI vs. CF_3SO_3) and, in particular, to the incorporation of $PYR_{14}TFSI$ on the conductivity of PEO-based electrolytes, especially at low–medium temperatures. The $P(EO)_{10}LiCF_3SO_3$ electrolyte exhibits a step increase at 60 °C that shifts down to 40 °C in the $P(EO)_{10}LiTFSI$ sample. On the other hand, the $P(EO)_{10}LiTFSI–PYR_{14}TFSI$ electrolyte shows a conductivity larger than 10⁻⁴ S cm⁻¹ at 20 °C which is two orders of magnitude higher than that of the RTIL-free sample and of interest

Table 1

Ionic conductivity and lithium anode/polymer electrolyte interface resistance values of $P(EO)_{10}LiCF_3SO_3$ (from Ref. [20]), $P(EO)_{10}LiTFSI$ [29] and $P(EO)_{10}LiTFSI–PYR_{14}TFSI$ [29] polymer electrolytes at different temperatures.

$t/°C$	$P(EO)_{10}LiCF_3SO_3$	$P(EO)_{10}LiTFSI$	$P(EO)_{10}LiTFSI–PYR_{14}TFSI$
Ionic conductivity/S cm^{-1}			
20	8.0×10^{-8}	1.3×10^{-6}	1.1×10^{-4}
30	1.9×10^{-7}	1.0×10^{-5}	2.6×10^{-4}
40	5.1×10^{-7}	1.0×10^{-4}	4.9×10^{-4}
50	9.0×10^{-7}	2.0×10^{-4}	7.9×10^{-4}
60	2.5×10^{-5}	3.5×10^{-4}	1.0×10^{-3}
70	6.7×10^{-5}	5.8×10^{-4}	1.5×10^{-3}
80	1.2×10^{-4}	8.4×10^{-4}	1.9×10^{-3}
90	1.6×10^{-4}	1.0×10^{-3}	2.2×10^{-3}
Lithium anode-polymer electrolyte interfacial resistance/Ω cm^2			
20	n.a.	1300	780
25	n.a.	600	380
30	n.a.	440	280
35	n.a.	330	230
40	n.a.	280	200

for practical applications. At 50 °C, the conductivity of the RTIL-containing sample is seen to approach 10^{-3} S cm^{-1}. In Table 1 are also reported the lithium anode/polymer electrolyte interface resistance values at different temperatures [29]. It is interesting to notice that the addition of $PYR_{14}TFSI$ leads to an interfacial resistance decrease, e.g., from 60% to 70%, in the whole temperature range investigated. This effect is likely to be ascribed to the presence of ionic liquid at the lithium anode/polymer electrolyte interface and/or its fragments in the passive layer (also called SEI) [34] formed with RTIL-based electrolytes. Therefore, the presence of ionic liquid in the SEI may promote the mobility of Li$^+$ cation through the passive layer, resulting in a faster Li$^+$ charge transfer at Li/SPE interface, e.g., lower interfacial resistance. It is to note that this approach might be the key for overcoming the Li/SPE interfacial resistance drawback in LMPBs. However, this mechanism needs to be further clarified and efforts are still needed to identify suitable and/or tune RTILs to further improve the behavior at the Li metal/polymer electrolyte interface.

The results of the chemical and electrochemical stability measurements are illustrated in Fig. 1. Panel A reports the high frequency region of the impedance responses taken (at 20 °C) on a symmetrical Li/$P(EO)_{10}LiTFSI–PYR_{14}TFSI$/Li cell as assembled and after a 253 days storage time. The intercept of the AC responses with the real axis corresponds to the electrolyte resistance [34]. No feature change of the AC plot of the RTIL-containing polymer electrolytes was observed even after such a prolonged storage time. This indicates that no phase separation and/or syneresis phenomenon (i.e., ionic liquid leakage) takes place in the material, thus supporting for the high chemical stability of the ternary electrolyte system even in contact with lithium metal. It is to note that $P(EO)_{10}LiTFSI–PYR_{14}TFSI$ films appeared very homogeneous even after prolonged storage times, e.g., more than one year. Panel B compare the LSV trace obtained for a $P(EO)_{10}LiTFSI–PYR_{14}TFSI$ electrolyte (solid line) and a RTIL-free $P(EO)_{10}LiTFSI$ sample (dotted line), respectively. The addition of ionic liquid does not deplete the electrochemical stability of the PEO electrolytes that exhibited an ESW from the lithium plating to about 4.9 V vs. Li/Li$^+$ at 20 °C. It is to note that the larger current increases, detected prior the anodic or cathodic breakdowns in the $P(EO)_{10}LiTFSI–PYR_{14}TFSI$ sample with respect to a RTIL-free $P(EO)_{10}LiTFSI$ one, are due to the much higher ionic conductivity of the former electrolyte (Table 1). A very low current flow (<10 μA cm^{-2}) was observed up to the anodic breakdown voltage, thus supporting for the high purity of the RTIL-based polymer electrolytes. On the cathodic verse, three weak ($\leq$20 μA cm^{-2}) peaks are observed around 1.3 V, 0.5 V and 0.25 V vs. Li/Li$^+$, respectively. Analogous behavior was exhibited from other RTIL-based polymer electrolytes [35,36]. From data
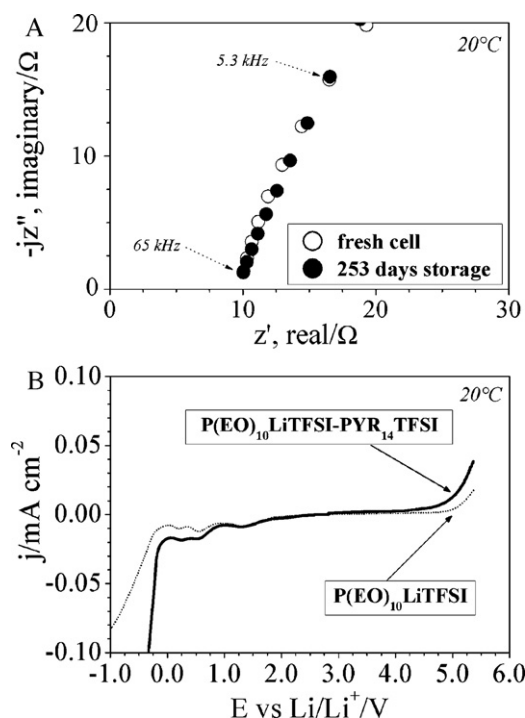

Fig. 1. Panel A: high frequency region of the AC response of a Li/$P(EO)_{10}LiTFSI–PYR_{14}TFSI$/Li cell taken at different storage times. Frequency range: 65 kHz–10 mHz. t = 20 °C. Panel B: electrochemical stability window of $P(EO)_{10}LiTFSI$ (dotted line) and $P(EO)_{10}LiTFSI–PYR_{14}TFSI$ (solid line) polymer electrolytes at 20 °C. Nickel as working electrode. Lithium as counter and reference electrodes, respectively. Scan rate: 0.5 mV s^{-1}.

reported in literature, we can assign the peaks at 1.3 V and 0.5 V vs. Li/Li$^+$ to the more or less reversible intercalation process of Li$^+$ cations into the native Ni$_x$O film on the nickel working electrode surface [37] whereas the feature at 0.25 V vs. Li/Li$^+$ is likely due to impurities.

3.2. Li/LiFePO$_4$ full polymer batteries

The performance of the Li/$P(EO)_{10}LiTFSI–PYR_{14}TFSI$/LiFePO$_4$ polymer batteries was evaluated as a function of the temperature at various current rates from C/50 to 2C and compared with that of the RTIL-free LMPBs (Li/$P(EO)_{10}LiTFSI$/LiFePO$_4$).

Fig. 2 depicts the voltage/capacity profile (current rates equal to C/20) of the 1st discharge half-cycles (panel A) and the cycling performance (panel B), obtained at 20 °C and 30 °C, of RTIL-containing (solid line) and RTIL-free (dotted line) Li/SPE/LiFePO$_4$ batteries. The comparison of the results shows clearly the beneficial effect due to the incorporation of ionic liquids on the room temperature battery performance. As expected, RTIL-free batteries deliver just a very modest capacity, i.e., 5 mA h g^{-1} and 10 mA h g^{-1}, respectively, at 20 °C and 30 °C, thus once more highlighting the extremely poor performance of these LMPBs at room temperature. Conversely, RTIL-incorporating batteries are able to deliver the theoretical capacity (170 mA h g^{-1}) at 30 °C and still a capacity of 115 mA h g^{-1} at 20 °C, which quickly levels at 90 mA h g^{-1}. In addition, the Li/$P(EO)_{10}LiTFSI–PYR_{14}TFSI$/LiFePO$_4$ LMPBs show an excellent capacity retention with a coulombic efficiency close to 100%. The relevant improvement due to RTIL incorporation is also highlighted by the flat plateau (Li insertion process) in the 3.4–3.2 V range, typical of Li/SPE/LiFePO$_4$ batteries [38,39], this indicating that RTIL-incorporating LMPBs are capable of maintaining the same voltage during almost the entire discharge step. Finally, the remarkable reduction of ohmic drop that occurs in RTIL-
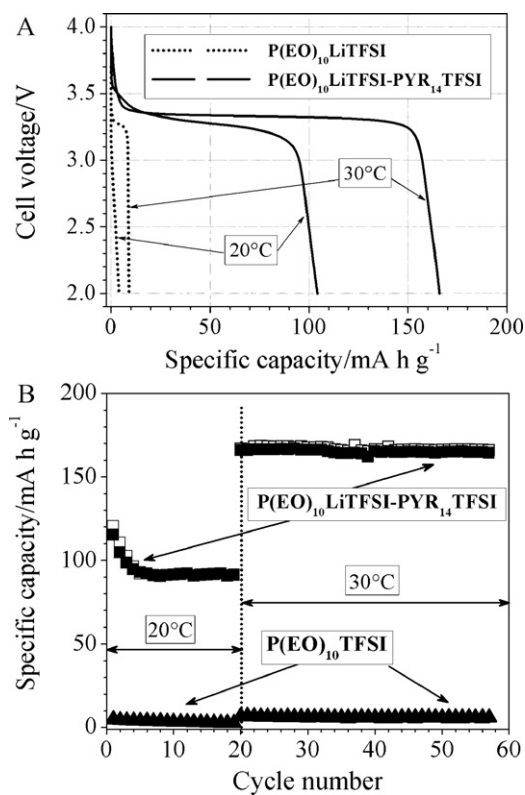
Fig. 2. Voltage vs. capacity profile of the 1st discharge half-cycles (panel A) and cycling performance (panel B), obtained at 20 °C and 30 °C, of RTIL-free Li/P(EO)$_{10}$LiTFSI/LiFePO$_4$ (dotted lines and triangles) and RTIL-incorporating Li/P(EO)$_{10}$LiTFSI–PYR$_{14}$TFSI/LiFePO$_4$ (solid lines and squares) polymer batteries. Current rates: C/20. Charge step: open data markers. Discharge step: solid data markers.
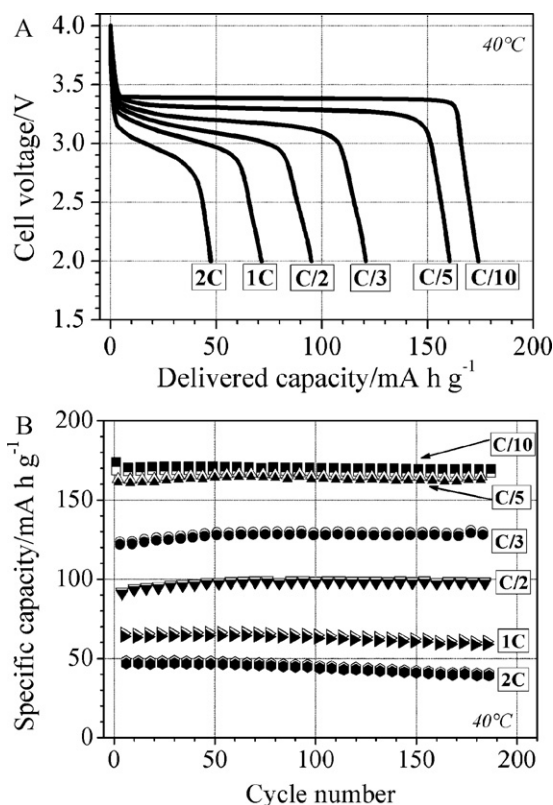

Fig. 3. Voltage vs. capacity profile of selected discharge half-cycles (panel A) and cycling performance (panel B), obtained at different current rates, for RTIL-incorporating Li/P(EO)$_{10}$LiTFSI–PYR$_{14}$TFSI/LiFePO$_4$ polymer batteries. $t = 40$ °C. Charge step: open data markers. Discharge step: solid data markers.

containing batteries, especially at 20 °C, supports once more for the much higher ionic conductivity of ionic liquid-based polymer electrolytes, in very good agreement with the results of Table 1. These very promising results indicate the feasibility of RTIL-incorporating lithium polymer batteries for high safety, room temperature applications.

The performance of Li/P(EO)$_{10}$LiTFSI–PYR$_{14}$TFSI/LiFePO$_4$ polymer batteries was also investigated at 40 °C as reported in Fig. 3. Panel A illustrates the voltage vs. capacity profile of selected discharge half-cycles obtained at various current rates, revealing a well-defined voltage curve and a moderate ohmic drop up to medium discharge rates (C/3). The results plotted in Panel B show a very good cycling behavior with large capacities up to medium rates, e.g., 170 mA h g^{-1}, 160 mA h g^{-1}, 125 mA h g^{-1} and 95 mA h g^{-1} were discharged at C/10, C/5, C/3 and C/2, respectively. In addition, interesting values are delivered also at high rates, e.g., about 75 mA h g^{-1} and 50 mA h g^{-1} at 1C and 2C, respectively. Above 93% of the initial capacity is still discharged after about 200 charge/discharge cycles run within the full voltage range (corresponding to 100% DOD at lower rates), thus highlighting the excellent capacity retention. This and the 100% coulombic efficiency achievement are certainly related to the very good electrolyte (IL-containing)/electrode compatibility, which results from the high purity materials and the cell manufacturing besides high stability cathode material. Therefore, RTIL-based LMPBs operating at 40 °C are appealing candidates for high energy density applications such as electric vehicles and, even better, renewable power sources.

From a comparison with analogous Li/P(EO)$_{10}$LiTFSI–PYR$_{14}$TFSI/LiFePO$_4$ cells preliminarily investigated [30], the optimized LMPBs show enhanced performance in terms of capac-

ity, rate capability and cycle life as well as electrolyte/electrode interfacial resistance (Fig. 5). This is likely addressed to both the superior quality of the LiFePO$_4$ cathode active material (e.g., lower particle size) and any technologic improvements as:

(i) drying process of ionic liquids run under high vacuum that reduced the water content down to 1 ppm. This issue has allowed an improvement of the electrolyte/electrode interface, particularly with lithium anode, thus reducing the overall cell impedance;
(ii) optimized manufacturing process that allowed a better evacuation of the laminated, vacuum-sealed cells, thus improving the behavior at the electrolyte/electrode interface.

Fig. 4 summarizes the discharge capacity vs. temperature behavior of Li/P(EO)$_{10}$LiTFSI–PYR$_{14}$TFSI/LiFePO$_4$ polymer batteries at various current densities (see legend in the figure). The capacity values are also listed in Table 2. At 40 °C no relevant difference in capacity with the current density is noticed up to C/5 (0.13 mA cm^{-2}) where the ionic liquid-containing Li/LiFePO$_4$ polymer batteries are capable to deliver capacities exceeding 160 mA h g^{-1} (>94% of the theoretical value). More than 120 mA h g^{-1} are still provided at a discharge rate of C/3, which is of particular interest for EV applications, whereas an appreciable capacity (about 50 mA h g^{-1}) is discharged even at high rates (e.g., 2C corresponding to a current density of 1.3 mA cm^{-2}). A progressive capacity decay is observed with the decreasing of the temperature, especially at medium-high current rates. At 30 °C and 25 °C capacities higher than 133 mA h g^{-1} are discharged at C/10 (30 °C) and C/20 (20 °C), respectively whereas, at higher rates, discharge values above 70 mA h g^{-1} are observed up to C/5. Below 25 °C large capacities (>100 mA h g^{-1}) are delivered only at low

Table 2
Delivered capacity of Li/P(EO)$_{10}$LiTFSI–PYR$_{14}$TFSI/LiFePO$_4$ polymer batteries at different temperatures and current rates.

Current rate	Current density/mA cm^{-2}	Delivered capacity/mA h g^{-1}				
		20 °C	25 °C	30 °C	35 °C	40 °C
C/50	0.013	154.0	165.8	169.3	170.0	171.1
C/20	0.032	114.0	140.0	166.4	169.1	169.7
C/10	0.065	n.a.	104.1	133.4	160.2	168.4
C/5	0.130	n.a.	69.9	90.0	125.2	160.7
C/3	0.217	n.a.	42.9	60.9	87.5	121.9
C/2	0.325	n.a.	22.5	42.8	64.4	91.1
1C	0.650	n.a.	6.3	12.5	33.8	64.1
2C	1.300	n.a.	2.4	5.1	11.6	46.8

rates, i.e., 154 mA h g^{-1} (C/50) and 114 mA h g^{-1} (C/20) are provided at 20 °C, respectively. Conversely, appreciable capacities are delivered at high rates (>1C) only above 35 °C. This behavior suggests that the battery performance is governed by two separate phenomena as the electrolyte/electrode charge transfer (at high rates) and the lithium diffusion in the composite cathode (at low rates). Both phenomena are mitigated by a temperature increase, this resulting in increased delivered capacities.

In order to investigate the reason of the performance decay at near room temperature, impedance measurements were carried out on Li/P(EO)$_{10}$LiTFSI–PYR$_{14}$TFSI/LiFePO$_4$ full batteries at temperatures ranging from 20 °C to 40 °C. The AC responses (panel A of Fig. 5) show a semicircle (associated with the overall electrode/electrolyte interfacial resistances [34]) followed (low frequency region) by a 45° linear portion and, then, an inclined straight line towards the real axes, Z′, that account on the bulk electrolyte diffusion, i.e., Warburg impedance [34] (not evidenced in the figure) and on the cathode limit capacitance [34], respectively. The high-frequency intercept of the semicircle with the real axes gives the electrolyte ionic resistance [34]. The shape of the impedance responses (normalized with respect to the electrochemical active area), typical of Li/polymer electrolyte/cathode cells, does not substantially change with the temperature. However, a substantial reduction of the semicircle, which corresponds to a battery impedance decrease, is observed on progressively increasing the cell temperature from 20 °C to 40 °C, particularly above 30 °C. Panel B of Fig. 5 plots the overall resistance vs. temperature dependence of a P(EO)$_{10}$LiTFSI–PYR$_{14}$TFSI full battery. The data were obtained analyzing the impedance responses depicted in panel A by a non-linear least-square (NLLSQ) fit software [40,41] using the
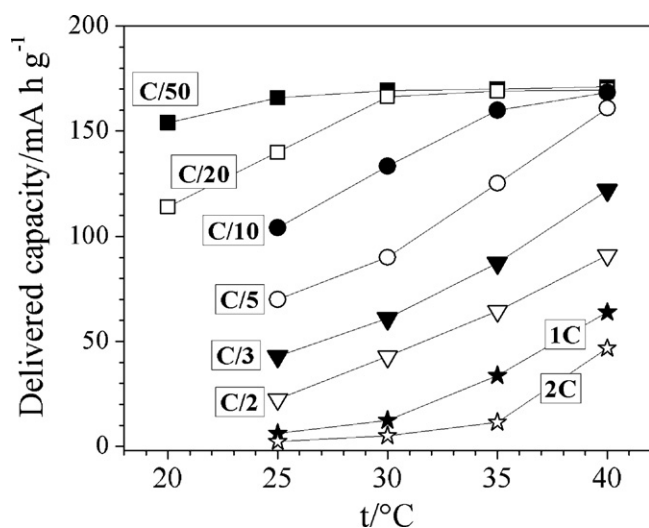
equivalent circuit model [34] reported in Fig. 6B. The discharge capacity vs. temperature dependence (obtained at C/20) is reported in panel B for comparison purpose. The full battery impedance increases almost linearly on decreasing temperature displaying a steeper raise below 30 °C whereas the temperature dependence of the Li/LiFePO$_4$ battery discharge capacity shows an opposite trend. This clearly indicates that the performance decay at low temperatures is most likely associated to the strong increase of the battery resistance below 30 °C.

Impedance measurements were also performed on symmetrical LiFePO$_4$/P(EO)$_{10}$LiTFSI–PYR$_{14}$TFSI/LiFePO$_4$ cells at 20 °C and 40 °C (panel A of Fig. 7). The high frequency region is magnified in the insert of panel A. With respect to the Li/P(EO)$_{10}$LiTFSI–PYR$_{14}$TFSI/LiFePO$_4$ full batteries (depicted in the same panel for comparison purpose), the AC plots of the LiFePO$_4$/LiFePO$_4$ cells, fitted with the above NLLSQ fit software
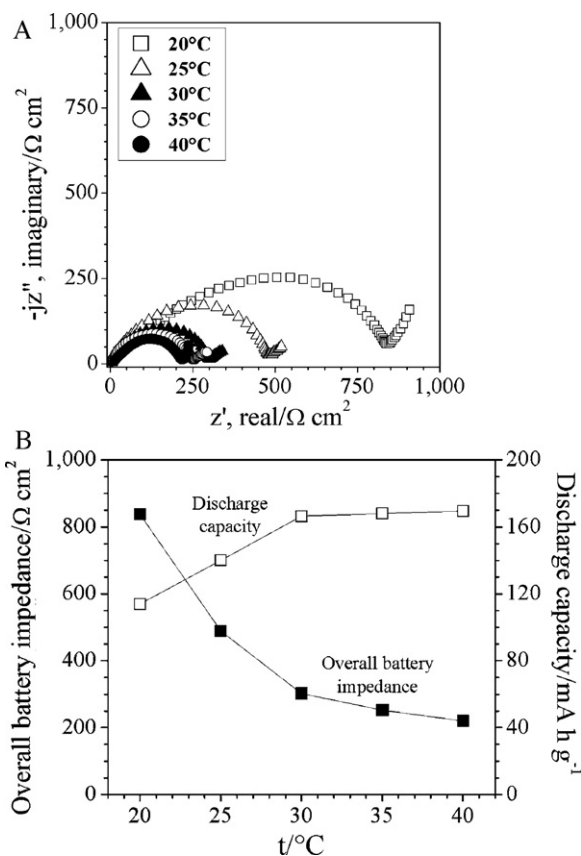

Fig. 5. AC response (normalized with respect to the electrochemical active area) evolution (panel A) and overall battery impedance (panel B) as a function of the temperature for a Li/P(EO)$_{10}$LiTFSI–PYR$_{14}$TFSI/LiFePO$_4$ polymer battery. Frequency range: 10 kHz–10 mHz. The discharge capacity (open data markers) vs. temperature plot is also reported in panel B.
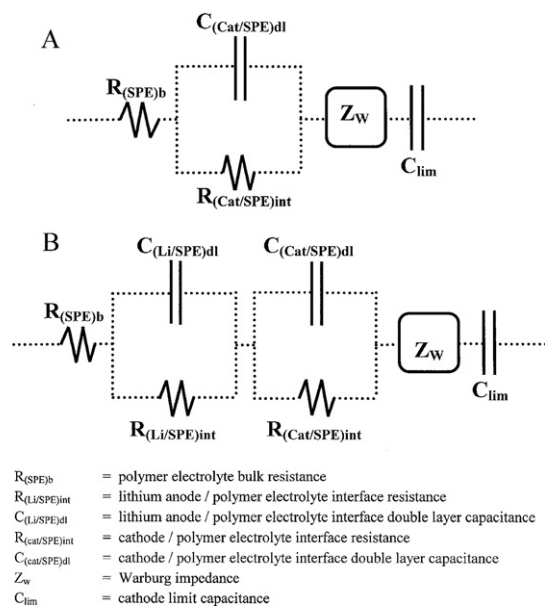

Fig. 4. Discharge capacity vs. temperature plot of Li/P(EO)$_{10}$LiTFSI–PYR$_{14}$TFSI/LiFePO$_4$ polymer batteries tested at various current densities.

R$_{(SPE)b}$ = polymer electrolyte bulk resistance
R$_{(Li/SPE)int}$ = lithium anode / polymer electrolyte interface resistance
C$_{(Li/SPE)dl}$ = lithium anode / polymer electrolyte interface double layer capacitance
R$_{(cat/SPE)int}$ = cathode / polymer electrolyte interface resistance
C$_{(cat/SPE)dl}$ = cathode / polymer electrolyte interface double layer capacitance
Z$_w$ = Warburg impedance
C$_{lim}$ = cathode limit capacitance

Fig. 6. Equivalent circuit model used to analyze the raw impedance data of the LiFePO$_4$/P(EO)$_{10}$LiTFSI–PYR$_{14}$TFSI/LiFePO$_4$ symmetrical cells (panel A) and Li/P(EO)$_{10}$LiTFSI–PYR$_{14}$TFSI/LiFePO$_4$ full batteries (panel B). The circuital parameters are indicated in the legend.

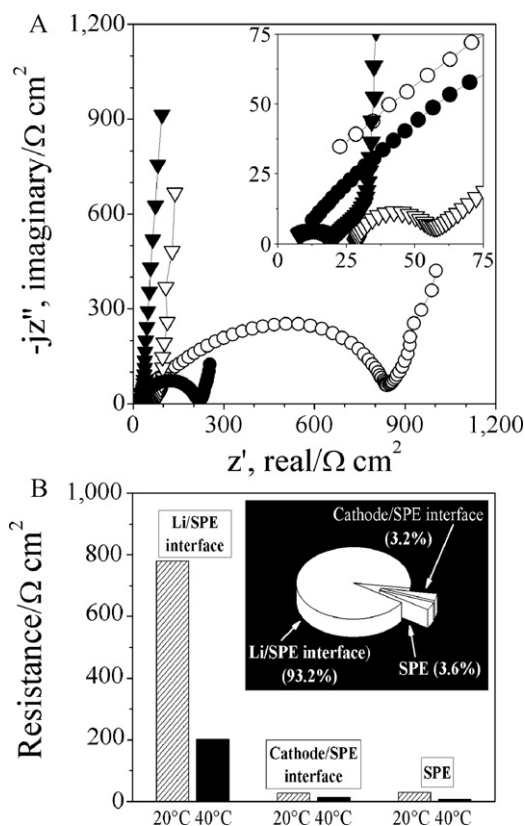**Fig. 7.** Panel A: AC response (normalized with respect to the electrochemical active area) of Li/P(EO)$_{10}$LiTFSI–PYR$_{14}$TFSI/LiFePO$_4$ polymer batteries (circles) and LiFePO$_4$/P(EO)$_{10}$LiTFSI–PYR$_{14}$TFSI/LiFePO$_4$ symmetrical cells (triangles) at 20 °C (open data markers) and 40 °C (solid data markers). The insert magnifies the high frequency region. Panel B: interfacial and electrolyte resistance values in a Li/P(EO)$_{10}$LiTFSI–PYR$_{14}$TFSI/LiFePO$_4$ polymer battery at 20 °C and 40 °C. The percent value of each contribute to the overall battery impedance is depicted in the insert of panel B.

using the equivalent circuit model reported in Fig. 6A, show very similar feature (a semicircle followed by a 45° linear portion and, successively, an inclined straight line towards the real axes) and electrolyte bulk resistance (high-frequency intercept of the semicircle with the real axes [34]). No substantial shape change with the temperature was detected whereas a relevant reduction of the semicircle (associated with the overall interfacial resistance [34]) is observed on passing from 20 °C to 40 °C. However, from the comparison with the response of Li/LiFePO$_4$ cells, the LiFePO$_4$/LiFePO$_4$ cells show a drastic reduction of the semicircle and, therefore, of the overall cell impedance (i.e., more than one order of magnitude). This clearly indicates that the LiFePO$_4$/SPE interfacial resistance results remarkably lower than that at the Li/SPE interface. The resistance contribution in a Li/LiFePO$_4$ polymer battery were evaluated by analyzing the AC plots reported in panel A of Fig. 7 using the software mentioned above [40,41]. The impedance responses taken on the symmetrical LiFePO$_4$/LiFePO$_4$ polymer cells were fitted to evaluate the LiFePO$_4$/SPE interface resistance that is in very good agreement with the values obtained from analysis of the Li/LiFePO$_4$ battery AC plots. The results, illustrated in panel B of Fig. 7, show clearly that both the LiFePO$_4$/SPE interface resistance (e.g., 26 Ω cm^2 and 12.5 Ω cm^2 at 20 °C and 40 °C, respectively) and the polymer electrolyte resistance (e.g., 30 Ω cm^2 and 6.5 Ω cm^2 at 20 °C and 40 °C, respectively) are almost negligible with respect to the resistance of the Li/SPE interface (e.g., 780 Ω cm^2 and 200 Ω cm^2 at 20 °C and 40 °C, respectively). This means that the overall resistance in lithium metal polymer batteries is almost fully associated to the Li/SPE interface (e.g., above 93%) as shown in the insert of panel B. Therefore, the performance battery decay observed below 30 °C has to be addressed mostly to the Li/SPE resistance.

4. Conclusions

The incorporation of RTILs such as N-butyl-N-methylpyrrolidinium bis(trifluoromethanesulfonyl)imide, PYR$_{14}$TFSI, into PEO–LiX polymer electrolytes allows to reduce the operative temperature of LMPBs down to room temperature without depleting the chemical/electrochemical properties.

All-solid-state, solvent-free Li/LiFePO$_4$ polymer batteries based on PYR$_{14}$TFSI RTIL are able to deliver the theoretical capacity (170 mA h g^{-1}) at 30 °C and still large capacities (>100 mA h g^{-1}) at 20 °C with excellent cycle capability and coulombic efficiency close to 100% at 100% of DOD. At 40 °C large capacities are discharged even at medium rates (e.g., 125 mA h g^{-1} at C/3).

The performance decay below 30 °C is almost fully ascribed to the remarkable increase of the resistance at Li/SPE interface, that represents more than 93% of the overall battery impedance. A further development of LMPBs will strongly depend on the improvement of the lithium/polymer electrolyte interface that represents the bottleneck for room temperature applications. Very important to notice, however, is that the incorporation of the RTILs improves the Li/SPE interfacial properties. Although the observed improvement is limited to a resistance decrease of about 30%, it certainly supports for the search of tailored ILs, which would be able to decrease the Li/SPE interface resistance further.

References

[1] B. Scrosati, Nature 373 (1995) 557.
[2] S.P. Beaton, G.A. Bishop, Y. Ziang, L.L. Ashbaugh, D.R. Lawson, D.H. Stedman, Science 268 (1995) 991.
[3] F.R. Kalhammer, A. Kozawa, C.B. Moyer, B.B. Owens, Electrochem. Soc. Interface 5 (1996) 32.
[4] J. Aragane, K. Matsui, H. Andoh, S. Sukuki, H. Fukuda, H. Ikeaya, K. Kitaba, R. Ishikawa, J. Power Sources 68 (1997) 13.
[5] J.M. Tarascon, M. Armand, Nature (London) 414 (2001) 359.
[6] M. Armand, J.M. Chabagno, M.J. Duclot, in: P. Vashishta, J.N. Mundy, G.K. Shenoy (Eds.), Fast Ion Transport in Solid, Elsevier, New York, 1989.
[7] P. Lightfoot, M.A. Metha, P.G. Bruce, Science 262 (1993) 883.
[8] C.A. Vincent, B. Scrosati, Modern Batteries. An Introduction to Electrochemical Power Sources, 2nd ed., Arnold, London, 1993.
[9] F.M. Gray, Polymer Electrolytes, Royal Society of Chemistry Monographs, Cambridge, 1997.
[10] F.M. Gray, M. Armand, in: T. Osaka, M. Datta (Eds.), Energy Storage System for Electronics, Gordon and Breach, Amsterdam, 2000.
[11] W. Wieczorek, K. Such, H. Wycislik, J. Plocharski, Solid State Ionics 36 (1989) 225.
[12] M.C. Borghini, M. Mastragostino, S. Passerini, B. Scrosati, J. Electrochem. Soc. 142 (1995) 2118.
[13] G.B. Appetecchi, S. Scaccia, S. Passerini, J. Electrochem. Soc. 147 (2000) 4448.
[14] G.B. Appetecchi, F. Alessandrini, R.G. Duan, A. Arzu, S. Passerini, J. Power Sources 1 (2001) 4335.
[15] R. Frech, S. Chintapalli, P.G. Bruce, C.A. Vincent, Macromolecules 32 (1999) 808.
[16] V. Rossi Albertini, G.B. Appetecchi, R. Caminiti, F. Cillocco, F. Croce, C. Sadun, J. Macromol. Sci. Phys. B36 (1997) 629.
[17] S. Lascaud, M. Perrier, A. Valle, C. Besner, J. Prud'homme, M. Armand, Macromolecules 27 (1994) 7469.
[18] G.B. Appetecchi, W. Henderson, P. Villano, M. Berrettoni, S. Passerini, J. Electrochem. Soc. 148 (2001) 1171.
[19] G. Feuillade, P. Perche, J. Appl. Electrochem. 5 (1975) 63.
[20] G.B. Appetecchi, F. Alessandrini, M. Carewska, T. Caruso, P.P. Prosini, S. Scaccia, S. Passerini, J. Power Sources 97 (2001) 790.
[21] D.R. MacFarlane, J. Sun, M. Forsyth, P. Meakin, N. Amini, J. Phys. Chem. B 103 (1999) 4164.
[22] D.R. MacFarlane, J. Huang, M. Forsyth, Nature (London) 402 (1999) 792.
[23] J.-H. Shin, W.A. Henderson, S. Passerini, Electrochem. Commun. 5 (2003) 1016.
[24] J.-H. Shin, W.A. Henderson, S. Passerini, Electrochem. Solid-State Lett. 8 (2005) 125.
[25] J.-H. Shin, W.A. Henderson, S. Passerini, J. Electrochem. Soc. 152 (2005) A978.
[26] J.-H. Shin, W.A. Henderson, G.B. Appetecchi, F. Alessandrini, S. Passerini, Electrochim. Acta 50 (2005) 3859.
[27] J.-H. Shin, W.A. Henderson, S. Scaccia, P.P. Prosini, S. Passerini, J. Power Sources 156 (2006) 560.
[28] J.-H. Shin, W.A. Henderson, C. Tizzani, S. Passerini, S.-S. Jeong, K.-W. Kim, J. Electrochem. Soc. 153 (9) (2006) A1649.
[29] G.-T. Kim, G.B. Appetecchi, F. Alessandrini, S. Passerini, J. Power Sources 171 (2007) 861.
[30] G.B Appetecchi, G.-T. Kim, M. Montanino, F. Alessandrini, S. Passerini, ECS Trans. 11 (2008) 119.
[31] G.B. Appetecchi, S. Scaccia, C. Tizzani, F. Alessandrini, S. Passerini, J. Electrochem. Soc. 153 (9) (2006) A1685.
[32] G.B. Appetecchi, M. Montanino, D. Zane, M. Carewska, F. Alessandrini, S. Passerini, Electrochim. Acta 54 (2009) 1325.
[33] G.B. Appetecchi, M. Carewska, F. Alessandrini, P.P. Prosini, S. Passerini, J. Electrochem. Soc. 147 (2000) 451.
[34] J.R. MacDonald (Ed.), Impedance Spectroscopy, John Wiley & Sons, New York, 1987.
[35] G.B. Appetecchi, G.T. Kim, M. Montanino, M. Carewska, R. Marcilla, D. Mecerreyes, I. De Meatza, J. Power Sources 195 (2010) 3668.
[36] G.T. Kim, G.B. Appetecchi, M. Carewska, M. Joost, A. Balducci, M. Winter, S. Passerini, J. Power Sources 195 (2010) 6130.
[37] S. Passerini, B. Scrosati, J. Electrochem. Soc. 141 (1994) 889.
[38] N. Ravel, J.B. Goodenough, S. Besner, M. Gauthier, M. Armand, in: Abstracts of the Electrochemical Society and the Electrochemical Society of Japan Meeting (Abstract 127), vol. 99-2, Honolulu, 1997.
[39] G.B. Appetecchi, J. Hassoun, B. Scrosati, F. Croce, F. Cassel, M. Salomon, J. Power Sources 124 (2003) 246.
[40] B.A. Boukamp, Solid State Ionics 18 (1986) 136.
[41] B.A. Boukamp, Solid State Ionics 20 (1986) 31.